The Astrophysical Journal Supplement Series, 207:38 (14pp), 2013 August doi:10.1088/0067-0049/207/2/38

INTERPLANETARY NETWORK LOCALIZATIONS OF KONUS SHORT GAMMA-RAY BURSTS

V. D. Pal'shin[1], K. Hurley[2], D. S. Svinkin[1], R. L. Aptekar[1], S. V. Golenetskii[1], D. D. Frederiks[1], E. P. Mazets [1,31], P. P. Oleynik[1], M. V. Ulanov[1], T. Cline [3,32], I. G. Mitrofanov[4], D. V. Golovin[4], A. S. Kozyrev[4], M. L. Litvak[4], A. B. Sanin[4], W. Boynton[5], C. Fellows[5], K. Harshman[5], J. Trombka[3], T. McClanahan[3], R. Starr[3], J. Goldsten[6], R. Gold[6], A. Rau[7], A. von Kienlin[7], V. Savchenko[8], D. M. Smith[9], W. Hajdas[10], S. D. Barthelmy[3], J. Cummings[11,12], N. Gehrels[3], H. Krimm[11,13], D. Palmer[14], K. Yamaoka[15], M. Ohno[16], Y. Fukazawa[16], Y. Hanabata[16], T. Takahashi[15], M. Tashiro[17], Y. Terada[17], T. Murakami[18], K. Makishima[19], M. S. Briggs[20], R. M. Kippen[14], C. Kouveliotou[21], C. Meegan[22], G. Fishman[21], V. Connaughton[20], M. Boër[23], C. Guidorzi[24], F. Frontera[24,25], E. Montanari[24,26], F. Rossi[24], M. Feroci[27], L. Amati[25], L. Nicastro[25], M. Orlandini[25], E. Del Monte[27], E. Costa[27], I. Donnarumma[27], Y. Evangelista[27], I. Lapshov[27], F. Lazzarotto[27], L. Pacciani[27], M. Rapisarda[27], P. Soffitta[27], G. Di Cocco[25], F. Fuschino[25], M. Galli[28], C. Labanti[25], M. Marisaldi[25], J.-L. Atteia[29], R. Vanderspek[30], and G. Ricker[30]

[1] Ioffe Physical Technical Institute, St. Petersburg, 194021, Russia; val@mail.ioffe.ru
[2] Space Sciences Laboratory, University of California, 7 Gauss Way, Berkeley, CA 94720-7450, USA
[3] NASA Goddard Space Flight Center, Greenbelt, MD 20771, USA
[4] Space Research Institute, 84/32, Profsoyuznaya, Moscow 117997, Russia
[5] Department of Planetary Sciences, University of Arizona, Tucson, AZ 85721, USA
[6] Applied Physics Laboratory, Johns Hopkins University, Laurel, MD 20723, USA
[7] Max-Planck-Institut für extraterrestrische Physik, Giessenbachstrasse, Postfach 1312, D-85748 Garching, Germany
[8] François Arago Centre, APC, Université Paris Diderot, CNRS/IN2P3, CEA/Irfu, Observatoire de Paris, Sorbonne Paris Cité, 10 rue Alice Domon et Léonie Duquet, F-75205 Paris Cedex 13, France
[9] Physics Department and Santa Cruz Institute for Particle Physics, University of California, Santa Cruz, Santa Cruz, CA 95064, USA
[10] Paul Scherrer Institute, CH-5232 Villigen PSI, Switzerland
[11] UMBC/CRESST/NASA Goddard Space Flight Center, Greenbelt, MD 20771, USA
[12] UMBC Physics Department, 1000 Hilltop Circle, Baltimore, MD 21250, USA
[13] Universities Space Research Association, 10211 Wincopin Circle, Suite 500, Columbia, MD 20144, USA
[14] Los Alamos National Laboratory, Los Alamos, NM 87545, USA
[15] Institute of Space and Astronautical Science (ISAS/JAXA), 3-1-1 Yoshinodai, Chuo-ku, Sagamihara, Kanagawa 252-5210, Japan
[16] Department of Physics, Hiroshima University, 1-3-1 Kagamiyama, Higashi-Hiroshima, Hiroshima 739-8526, Japan
[17] Department of Physics, Saitama University, 255 Shimo-Okubo, Sakura-ku, Saitama-shi, Saitama 338-8570, Japan
[18] Department of Physics, Kanazawa University, Kadoma-cho, Kanazawa, Ishikawa 920-1192, Japan
[19] Department of Physics, University of Tokyo, 7-3-1 Hongo, Bunkyo-ku, Tokyo 113-0033, Japan
[20] CSPAR and Physics Department, University of Alabama in Huntsville, Huntsville, AL 35899, USA
[21] Space Science Office, VP62, NASA Marshall Space Flight Center, Huntsville, AL 35812, USA
[22] Universities Space Research Association, 320 Sparkman drive, Huntsville, AL 35805, USA
[23] Observatoire de Haute Provence (CNRS), F-04870 Saint Michel l'Observatoire, France
[24] Physics Department, University of Ferrara, Via Saragat 1, I-44100 Ferrara, Italy
[25] INAF/Istituto di Astrofisica Spaziale e Fisica Cosmica di Bologna, via Gobetti 101, I-40129 Bologna, Italy
[26] Istituto IS Calvi, I-41034 Finale Emilia (MO), Italy
[27] INAF–Istituto di Astrofisica Spaziale e Fisica Cosmica, via Fosso del Cavaliere, I-00133 Rome, Italy
[28] ENEA-Bologna, Via Martiri Montesole 4, I-40129 Bologna, Italy
[29] Université de Toulouse; UPS-OMP; CNRS; IRAP; 14 Avenue Edouard Belin, F-31400 Toulouse, France
[30] Kavli Institute for Astrophysics and Space Research, Massachusetts Institute of Technology, 70 Vassar Street, Cambridge, MA 02139, USA
Received 2013 June 25; accepted 2013 July 11; published 2013 August 2

ABSTRACT

Between the launch of the *Global Geospace Science Wind* spacecraft in 1994 November and the end of 2010, the Konus-*Wind* experiment detected 296 short-duration gamma-ray bursts (including 23 bursts which can be classified as short bursts with extended emission). During this period, the Interplanetary Network (IPN) consisted of up to 11 spacecraft, and using triangulation, the localizations of 271 bursts were obtained. We present the most comprehensive IPN localization data on these events. The short burst detection rate, $\sim$18 yr^{-1}, exceeds that of many individual experiments.

Key words: catalogs – gamma-ray burst: general – techniques: miscellaneous

Online-only material: color figures, machine-readable tables

1. INTRODUCTION

Between 1994 November and 2010 December, the Konus gamma-ray spectrometer on board the *Global Geospace Science Wind* spacecraft detected 1989 cosmic gamma-ray bursts (GRBs) in the triggered mode, 296 of which were classified as short-duration GRBs or short bursts with extended emission (EE). The classification was made based on the duration distribution of an unbiased sample of 1168 Konus-*Wind* GRBs. The instrument trigger criteria cause undersampling of faint short bursts relative to faint long bursts, so this subsample of fairly bright (in terms of peak count rate in Konus-*Wind*'s trigger energy band) bursts has been chosen for the purpose of classification. Taking into account other characteristics of these short-duration bursts such as hardness ratio and spectral lag shows that

[31] Deceased.
[32] Emeritus.

about 16% of them can be in fact Type II (collapsar-origin), or at least their classification as Type I (merger-origin) is questionable (see Zhang et al. 2009 for more information on the Type I/II classification scheme). Nevertheless we consider here all 296 Konus-*Wind* short-duration and possible short-duration with EE bursts (hereafter we refer to them simply as Konus short bursts). Full details of the Konus-*Wind* GRB classification are given in D. S. Svinkin et al. (2013, in preparation).

Every short burst detected by Konus was searched for in the data of the spacecraft comprising the Interplanetary Network (IPN). We found that 271 (∼92%) of the Konus-*Wind* short GRBs were observed by at least one other IPN spacecraft, enabling their localizations to be constrained by triangulation.

The IPN contained between 3 and 11 spacecraft during this period. They were, in addition to Konus-*Wind*, *Ulysses* (the solar X-ray/cosmic gamma-ray burst instrument, GRB), in heliocentric orbit at distances between 670 and 3180 lt-s from Earth (Hurley et al. 1992); the *Near-Earth Asteroid Rendezvous* (*NEAR*) mission (the remote sensing X-ray/Gamma-Ray Spectrometer, XGRS; Trombka et al. 1999), at distances up to 1300 lt-s from Earth; *Mars Odyssey* (the Gamma-Ray Spectrometer (GRS) that includes two detectors with GRB detection capabilities, the gamma sensor head (GSH), and the High Energy Neutron Detector (HEND); Boynton et al. 2004; Hurley et al. 2006), launched in 2001 April and in orbit around Mars starting in 2001 October, up to 1250 lt-s from Earth (Saunders et al. 2004); the *Mercury Surface, Space Environment, Geochemistry, and Ranging* (*MESSENGER*) mission (the Gamma-Ray and Neutron Spectrometer, GRNS; Goldsten et al. 2007), en route to Mercury (in Mercury orbit since 2011 March), launched in 2004 August, but commencing full operation only in 2007, up to ∼700 lt-s from Earth (Gold et al. 2001; Solomon et al. 2007); the *International Gamma-Ray Astrophysics Laboratory* (*INTEGRAL*; the anti-coincidence shield (ACS) of the spectrometer SPI, SPI-ACS; Rau et al. 2005), in an eccentric Earth orbit at up to 0.5 lt-s from Earth; and in low Earth orbits, the *Compton Gamma-Ray Observatory* (*CGRO*; the Burst and Transient Source Experiment, BATSE; Fishman et al. 1992); *BeppoSAX* (the Gamma-Ray Burst Monitor, GRBM; Frontera et al. 1997; Feroci et al. 1997); the *Reuven Ramaty High Energy Solar Spectroscopic Imager* (*RHESSI*; Lin et al. 2002; Smith et al. 2002); the *High Energy Transient Explorer* (*HETE-2*; the French Gamma-Ray Telescope, FREGATE; Ricker et al. 2003; Atteia et al. 2003); the *Swift* mission (the Burst Alert Telescope, BAT; Barthelmy et al. 2005; Gehrels et al. 2004); the *Suzaku* mission (the Wide-band All-sky Monitor, WAM; Yamaoka et al. 2009; Takahashi et al. 2007); *AGILE* (the Mini-Calorimeter, MCAL, and Super-AGILE; Tavani et al. 2009); the *Fermi* mission (the Gamma-Ray Burst Monitor, GBM; Meegan et al. 2009); the *Coronas-F* solar observatory (Helicon; Oraevskii et al. 2002); the *Cosmos 2326* (Konus-A; Aptekar et al. 1998), *Cosmos 2367* (Konus-A2), and *Cosmos 2421*(Konus-A3) spacecraft; and the *Coronas-Photon* solar observatory (Konus-RF).

At least two other spacecraft detected GRBs during this period, although they were not used for triangulation and therefore were not, strictly speaking, part of the IPN. They are the *Defense Meteorological Satellite Program* (*DMSP*; Terrell et al. 1996, 1998; Terrell & Klebesadel 2004) and the *Stretched Rohini Satellite Series* (*SROSS*; Marar et al. 1994).

Here we present the localization data obtained by the IPN for 271 Konus-*Wind* short bursts observed by at least one other IPN spacecraft (s/c). In a companion paper, we present the durations, energy spectra, peak fluxes, and fluences of these bursts.

2. OBSERVATIONS

For each Konus short GRB, a search was initiated in the data of the IPN spacecraft. For the near-Earth spacecraft and *INTEGRAL*, the search window was centered on the Konus-*Wind* trigger time, and its duration was somewhat greater than the *Wind* distance from Earth. For the spacecraft at interplanetary distances, the search window was twice the light-travel time to the spacecraft if the event arrival direction was unknown, which was the case for most events. If the arrival direction was known, even coarsely, the search window was defined by calculating the expected arrival time at the spacecraft, and searching in a window around it.

The mission timelines and the number of Konus-*Wind* short GRBs observed by each mission/instrument are shown in Figure 1. In this study, the largest number of bursts detected by an IPN instrument, after Konus, was 139, detected by *INTEGRAL* (SPI-ACS).

Table 1 lists the 271 Konus-*Wind* short GRBs observed by the IPN. The first column gives the burst designation, "GRBYYYYMMDD_Tssssss", where YYYYMMDD is the burst date, and ssssss is the Konus-*Wind* trigger time (s UT) truncated to integer seconds (Note that, due to *Wind*'s large distance from Earth, this trigger time can differ by up to 6.1 s from the Earth-crossing time; see below). The next two columns give the burst date and Konus-*Wind* trigger time in the standard date and time formats. The "Type" column specifies the burst type following the classification given in D. S. Svinkin et al. (2013, in preparation). The types are: I (merger-origin), II (collapsar-origin), I/II (the type is uncertain), Iee (type I which shows EE), and Iee/II (the type is uncertain: Iee or II). The "Time Delay" column gives the propagation time delay from *Wind* to the Earth center and its 3σ uncertainty (calculated using the IPN localizations, presented in this catalog: see Section 6.3). The "Observed by" column lists the missions/instruments which observed the burst (detections by several instruments which are not part of the IPN have also been listed, namely COMPTEL on *CGRO*, *DMSP*, *Fermi* LAT, *MAXI* (*Monitor of All-sky X-ray Image*), and *SROSS*. The next two columns give the total number of IPN s/c and the number of the distant IPN s/c which observed the burst. The last column contains the comments.

During the period of consideration, four interplanetary s/c participated in the IPN: *Ulysses*, *NEAR*, *Mars Odyssey*, and *MESSENGER*. Of the 271 bursts listed in Table 1, 30 bursts were observed by two distant s/c, 102 by one distant s/c, and 139 were not observed by any distant s/c.

Seventeen Konus short bursts were precisely localized by instruments with imaging capabilities, namely, *Swift*-BAT, *HETE-2* (WXM and SXC), and *INTEGRAL* IBIS/ISGRI. For most of these bursts an X-ray afterglow has been detected; for some of them a redshift z has been determined based on the optical afterglow or host galaxy spectroscopy. We have used these bursts to verify our IPN triangulations (see Section 4.3).

3. METHODOLOGY

When a GRB arrives at two spacecraft with a delay δT, it may be localized to an annulus whose half-angle θ with respect to the vector joining the two spacecraft is given by

$$\cos\theta = \frac{c\delta T}{D} \quad (1)$$

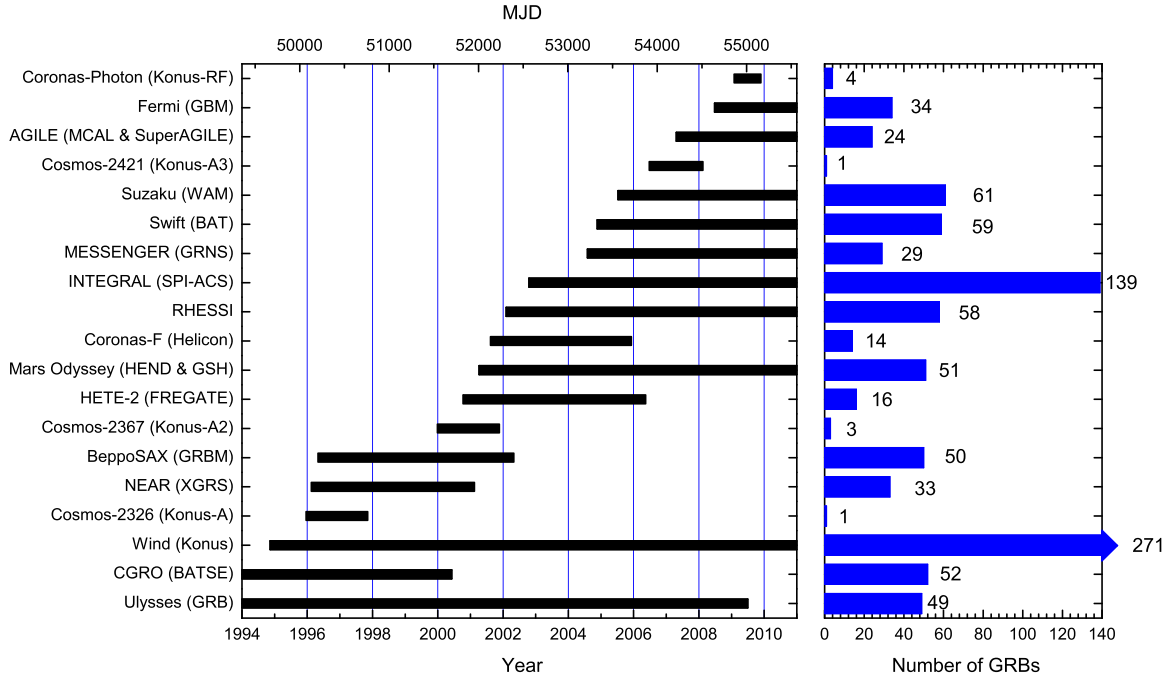

Figure 1. Left: timelines of the IPN missions since the launch of *Wind* in 1994 November (instrument names are given in the parentheses). Right: number of Konus short bursts observed by each mission (for *Wind* (Konus)—the number of bursts observed by at least one other IPN s/c is given).

(A color version of this figure is available in the online journal.)

Table 1
IPN/Konus Short Gamma-Ray Bursts

Designation	Date	Konus-*Wind* Trigger Time (UT)	Type	Time Delay[a] (s)	Observed by[b]	$N_{\rm tot}$	$N_{\rm dist}$	Note
GRB19950210_T08424	1995 Feb 10	02:20:24.148	I	−2.602(−0.009, +0.007)	Uly(T), GRO(#3410)	3	1	
GRB19950211_T08697	1995 Feb 11	02:24:57.749	I	0.003(−0.009, +0.005)	Uly(T), GRO(#3412), SRS(T)	4	1	
GRB19950414_T40882	1995 Apr 14	11:21:22.798	I	0.350(−0.008, +0.006)	Uly(R)	2	1	
GRB19950419_T08628	1995 Apr 19	02:23:48.860	I	0.418(−0.030, +0.026)	Uly(T)	2	1	
GRB19950523_T31302	1995 May 23	08:41:42.284	I	0.436(−0.068, +0.040)	Uly(T)	2	1	

Notes.

[a] Propagation time delay from *Wind* to the Earth center and its 3σ uncertainty. This delay should be added to the Konus-*Wind* trigger time to get the Earth-crossing time.

[b] AGI: *Astro-rivelatore Gamma a Immagini LEggero* (AGILE); GRO: *Compton Gamma-Ray Observatory (CGRO)*; COM: COMPTEL on *CGRO*; DMS: *Defense Meteorological Satellite Program*; Fer: *Fermi*; Hel: Helicon-*Coronas-F*; HET: *HETE-2*; INT: *International Gamma-Ray Laboratory (INTEGRAL)*; KA1: Konus-A on *Cosmos 2326*; KA2: Konus-A2 on *Cosmos 2367*; KA3: Konus-A3 on *Cosmos 2421*; KRF: Konus-RF on *Coronas-Photon*; LAT: *Fermi* Large Area Telescope; *MAXI*: *Monitor of All-sky X-ray Image*; MES: *Mercury Surface, Space Environment, Geochemistry, and Ranging* mission (*MESSENGER*); MO: *Mars Odyssey*; NEA: *Near Earth Asteroid Rendezvous* mission (*NEAR*); RHE: *Ramaty High Energy Solar Spectroscopic Imager (RHESSI)*; SAX: *BeppoSAX*; SRS: *Stretched Rohini Satellite Series* (*SROSS*); Suz: *Suzaku*; Swi: *Swift*; TGR: Transient Gamma-Ray Spectrometer (TGRS) on *Wind*; Uly: *Ulysses*. The detection mode is given in parentheses: T—trigger, R—rate increase; #n—trigger number (when available).

[1] Imaged by *HETE-2* (WXM and SXC).

[2] Imaged by *Swift*-BAT.

[3] Imaged by *INTEGRAL* IBIS/ISGRI.

(This table is available in its entirety in a machine-readable form in the online journal. A portion is shown here for guidance regarding its form and content.)

where c is the speed of light and D is the distance between the two spacecraft. (This assumes that the burst is a plane wave, i.e., that its distance is much greater than D.)

The measured time delay has an uncertainty which is generally not symmetrical $d_{\pm}(\delta T)$, i.e., the measured time delay can take values from $\delta T + d_{-}(\delta T)$ to $\delta T + d_{+}(\delta T)$ ($d_{-}(\delta T)$ is negative) at a given confidence level.

The annulus half-widths (HWs) $d\theta_{\pm}$, are

$$d\theta_{\pm} \equiv \theta_{\pm} - \theta = \cos^{-1}\left[\frac{c(\delta T + d_{\mp}(\delta T))}{D}\right] - \cos^{-1}\left[\frac{c\delta T}{D}\right]. \quad (2)$$

It should be noted that even in case of symmetrical errors $|d_{-}(\delta T)| = d_{+}(\delta T)$, the annulus can still be significantly asymmetrical if $c(\delta T + d_{\pm}(\delta T))/D \sim 1$ (i.e., the source is close to the vector joining the two spacecraft).

For the case $d(\delta T) \ll D/c$ Equation (2) reduces to the commonly used expression:

$$d\theta_{\pm} = -\frac{c d_{\mp}(\delta T)}{D \sin\theta}. \quad (3)$$

To derive the most probable time delay δT and its uncertainty $d_{\pm}(\delta T)$ we have used the χ^2 method described in Hurley et al. (1999a) for triangulations with distant s/c and this method

with some modifications for Konus-*Wind*–near-Earth s/c (or *INTEGRAL*) triangulations.

Given a burst time history recorded by two instruments, the most probable time lag τ and its uncertainty $d_{\pm}(\tau)$ can be estimated as follows. Let $n_{1,i} = n(t_{1,i})$, $n_{2,j} = n(t_{2,j})$ and $\sigma_{1,i}$, $\sigma_{2,j}$ denote background-subtracted counts and their uncertainties measured by two instruments at evenly spaced intervals $t_{1,i} = t_{01} + i\Delta_1$, $t_{2,j} = t_{02} + j\Delta_2$, where $i = 0, \ldots, m_1$, $j = 0, \ldots, m_2$; and Δ_1, Δ_2 are the bin sizes and t_{01}, t_{02} are the absolute reference times (UT). To make things simpler, suppose $\Delta_1 = \Delta_2 = \Delta$. Usually one assumes Poisson statistics, so $\sigma_{1(2),i} = n_{\mathrm{tot1(2)},i}^{1/2}$, where $n_{\mathrm{tot1(2)},i}$ is the total number of counts (source + background) in the ith bin. Let us assume that both time histories contain the burst of interest along with some intervals before and after it (if they do not exist they can always be added and padded with zeros with the background variance), and $N + 1$ bins from i_{start} contain the burst (or the part of the burst we want to cross-correlate) in the second time history. Let us construct the statistic:

$$R^2(\tau \equiv k\Delta) = \sum_{i=i_{\mathrm{start}}}^{i=i_{\mathrm{start}}+N} \frac{(n_{2,i} - s n_{1,i+k})^2}{\left(\sigma_{2,i}^2 + s^2\sigma_{1,i+k}^2\right)}, \quad (4)$$

where s is the scaling factor estimated as the ratio of the burst counts detected by the instruments $s = \sum_i n_{1,i} / \sum_j n_{2,j}$. In the perfect case of identical detectors, with identical energy ranges and arrival angles, and Poisson statistics, R^2 is distributed as χ^2 with N degrees of freedom (dof). In practice, there are several complicating factors. The detectors have different energy ranges, different responses, and operate in different background environments. Fortunately, for short GRBs some of these complicating factors are less important: (1) the background variation on short time scales is small, and (2) different spectral evolutions which produce a significant lag between light curves measured in different energy bands is almost absent in short GRBs (e.g., Norris et al. 2001).

To account for all deviations from the perfect case we adopt the following approach: for a given N (the number of bins used to construct R^2) we calculate $\chi^2(N)$ corresponding to the 3σ confidence level (that is, χ^2 for which the chi-square probability function $Q(\chi^2|N) = 2.7 \times 10^{-3}$), and adopt the corresponding 3σ level for the reduced $R_r^2 (\equiv R^2/N)$ of

$$R_{r,3\sigma}^2 = \chi_{r,3\sigma}^2(N) + R_{r,\min}^2 - 1, \quad (5)$$

where $R_{r,\min}^2$ is the minimum of $R_r^2(\tau)$; 1 is subtracted, since $R_{r,\min}^2 \sim 1$ for the perfect case (in practice it is often >1 and hence, $R_{r,3\sigma}^2 > \chi_{r,3\sigma}^2(N)$). To identify the 3σ confidence interval for τ, we use the nearest points of the $R_r^2(\tau)$ curve above the 3σ level given by Equation (5)—see the examples in Figure 2. After the time lag τ and its errors $d_{\pm}(\tau)$ have been found, the time delay and its uncertainty can be calculated as $\delta T = t_{02} - t_{01} + \tau$; $d_{\pm}(\delta T) = d_{\pm}(\tau)$ (here we assume there is no error in the absolute times t_{01} and t_{02}). For simplicity we will further refer to R^2 as χ^2.

4. LOCALIZATIONS: TRIANGULATION ANNULI

Using the above methodology one or more triangulation annuli have been obtained for 271 Konus-*Wind* short bursts. Specific details on the time delay determination for different pairs of instruments are given in the subsections below.

4.1. Annuli Involving Distant s/c

Distant (interplanetary) spacecraft play an important role in GRB triangulation. Their long baselines make it possible to derive very small error boxes for many bursts. However, the detectors on board these missions tend to be smaller than ones in orbits closer to Earth, and in some cases, are not dedicated GRB detectors, but rather, are planetary experiments which have GRB detection modes. Thus, they may have coarser time resolution and less sensitivity. Also, the spacecraft clocks on these missions are not always calibrated to UTC as accurately as the ones on missions closer to Earth (or their calibration cannot be determined as accurately). In the present catalog, the data of four interplanetary missions have been used: *Ulysses*, *NEAR*, *Mars Odyssey*, and *MESSENGER*. Of the four, only *Ulysses* had a dedicated GRB experiment. The time resolutions of the four ranged from 32 ms (*Ulysses*, triggered mode) to 1 s (*MESSENGER*, *NEAR*). When a short GRB is detected by an experiment with time resolution much greater than the burst duration, the result is usually an increase in the count rate in a single time bin, which means that the timing uncertainty is approximately one-half of the larger time resolution. The accuracy of the spacecraft clocks have been verified in two ways. For *Ulysses*, commands were sent to the GRB experiment at accurately known times, and, taking light-travel time and delays aboard the spacecraft into account, the timing could be verified to between several milliseconds and 125 ms. (Although we believe that the timing was accurate to several milliseconds, technical issues often prevented us from verifying it.) In addition, the timing of all the interplanetary missions can be verified using triangulation of transient sources whose positions are well known by other means: soft gamma-ray repeaters (SGRs) are one possibility, and GRBs localized by the *Swift* XRT or UVOT, for example, are another. For the purposes of this catalog, we have taken the extremely conservative approach that no 3σ cross-correlation uncertainty is less than 125 ms.

In total 132 Konus short bursts were observed by distant s/c: 30 by two distant s/c and 102 by one distant s/c. Among them nine were precisely localized by instruments with imaging capabilities. We do not give here distant s/c annuli for these nine bursts since they do not improve the precise localizations.

As a result 150 annuli have been obtained using the distant s/c data (two distant annuli for 27 bursts and one distant annulus for 96 bursts). Some of them have already been presented in the IPN catalogs: for BATSE bursts in Hurley et al. (1999a, 1999b, 2011b), for *BeppoSAX* bursts in Hurley et al. (2010a), and for *HETE-2* bursts in Hurley et al. (2011a).

The histogram of Figure 3 shows the distribution of 3σ HWs of these 150 annuli. The smallest HW is $0\overset{\circ}{.}0024$ ($0\overset{\prime}{.}14$), the largest is $2\overset{\circ}{.}21$, the mean is $0\overset{\circ}{.}099$ ($5\overset{\prime}{.}9$), and the geometrical mean is $0\overset{\circ}{.}028$ ($1\overset{\prime}{.}7$).

4.2. Annuli Involving Konus-Wind, INTEGRAL, and a Near-Earth s/c

The Konus-*Wind* (hereafter *KW*) experiment plays a special role in the IPN thanks to its unique set of characteristics: continuous coverage of the full sky by two omnidirectional spectrometers, orbit in interplanetary space that provides an exceptionally stable background, wide energy range (10 keV–10 MeV nominal; ~20 keV–15 MeV at the present time), and a rather high sensitivity of about 10^{-7} erg cm^{-2}. The *KW* duty cycle, defined as the time for data recovered divided by the total operational time of the experiment, is about 95%. It has observed most of

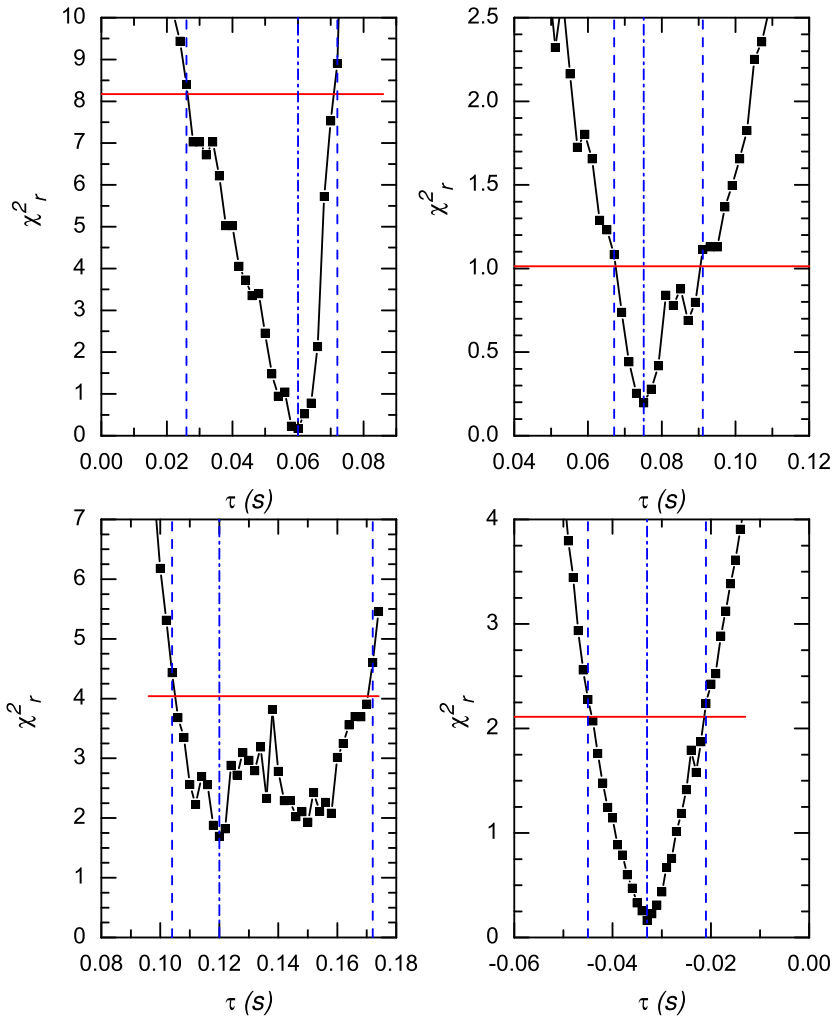

Figure 2. Examples of cross-correlation curves $\chi^2_r(\tau)$. Horizontal red lines denote 3σ levels. Vertical blue lines show the best cross-correlation time lag τ (dashed-dotted line) and its 3σ confidence interval (dashed lines). Top left: GRB19971118_T29008. Cross-correlation of the *KW* 2 ms light curve with the BATSE 64 ms light curve; $\tau = 0.060(-0.034, +0.012)$ s (dof = 2). Top right: GRB20070321_T67937. Cross-correlation of the *KW* 2 ms light curve with the WAM 1/64 s light curve; $\tau = 0.075(-0.008, +0.016)$ s (dof = 12). Bottom left: GRB20090715_T62736. Cross-correlation of the *KW* 2 ms light curve with the SPI-ACS 50 ms light curve; $\tau = 0.120(-0.016, +0.052)$ s (dof = 7). Bottom right: GRB20100206_T48606. Cross-correlation of the GBM 1 ms light curve with the *KW* 16 ms light curve; $\tau = -0.033 \pm 0.012$ s (dof = 9).

(A color version of this figure is available in the online journal.)

the IPN events, providing an important vertex in the IPN at a distance of $\simeq$1–7 lt-s (see Figure 4).

In the triggered mode *KW* records a burst time history in three energy ranges, G1, G2, G3, with nominal bounds 10–50 keV, 50–200 keV, and 200–750 keV, with a variable time resolution from 2 ms up to 256 ms (for more details see Aptekar et al. 1995). The time interval with the finest time resolution of 2 ms runs from $T_0 - 0.512$ s to $T_0 + 0.512$ s (T_0 is the trigger time) and in most cases covers the whole short burst, or at least its most intense pulse, thereby allowing very accurate cross-correlation with light curves of other instruments.

The *KW* clock is accurate to better than 1 ms, and this accuracy has been extensively verified by triangulation of many SGR bursts and GRBs.

The best results for cross-correlation with *KW* (i.e., minimum uncertainties in derived time delays) are provided by near-Earth s/c with high effective areas, namely *CGRO* BATSE, *BeppoSAX* GRBM, *INTEGRAL*-SPI-ACS, *Suzaku*-WAM, *Swift*-BAT, and *Fermi*-GBM.

At present, triangulation with *Fermi*-GBM usually provides the best result (the narrowest annulus) thanks to the similar designs of the *KW* and GBM detectors (NaI(Tl) scintillators), the high effective area of the GBM (several hundred cm^2 for the combination of several NaI(Tl) detectors), and photon time-tagging in 128 energy channels, which allows GBM light curves to be obtained in the same energy ranges as *KW* light curves with any desired time binning.

Since the clocks of most of the near-Earth instruments are very accurate, high count statistics combined with fine time resolution often results in an uncertainty in time delays as low as several milliseconds. Therefore, despite the rather small distance between *KW* and near-Earth s/c of several lt-s, the resulting relative error in time delay, $d_{\pm}(\delta T)/D$, which determines the width of the annulus (see Equations (2) and (3)) can be comparable to or sometimes even smaller than for annuli involving distant s/c. Such small uncertainties of several ms, and hence narrow annuli, can often be derived for short bursts with sharp peaks or very fast rise and/or decay times. On the other hand, bursts with smooth single-pulse light curves usually give rather large cross-correlation uncertainties in time delays, and hence, rather wide triangulation annuli.

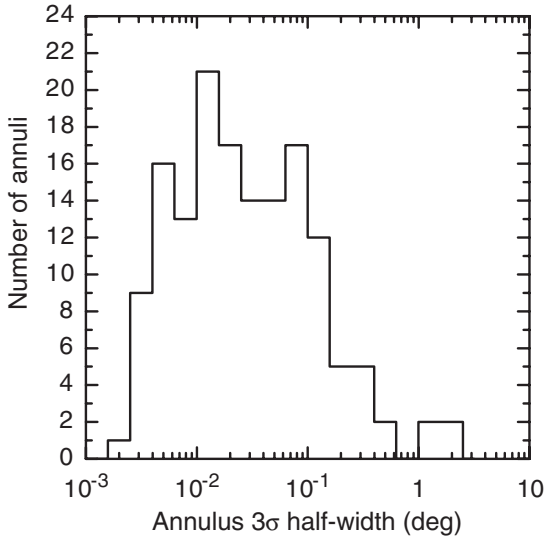

Figure 3. Distribution of 3σ half-widths (HWs) of the 150 triangulation annuli obtained using the distant s/c data. The smallest HW is 0.°0024 (0.′14), the largest is 2.°21, the mean is 0.°099 (5.′9), and the geometrical mean is 0.°028 (1.′7).

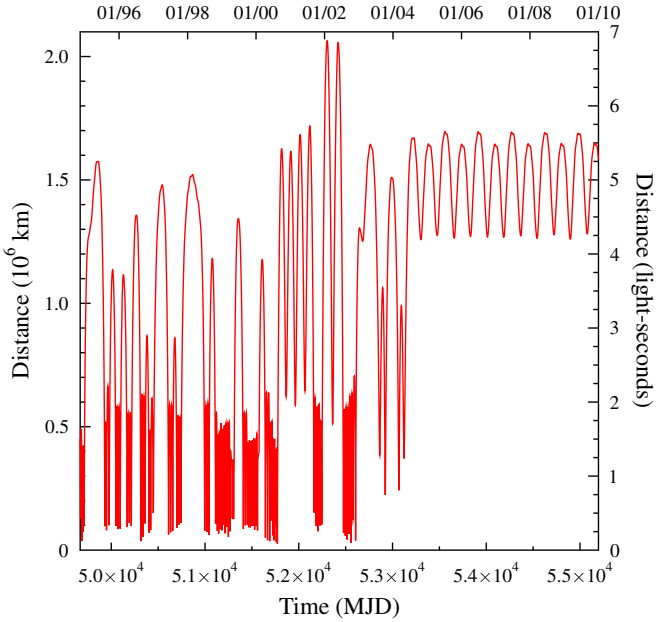

Figure 4. *Wind* distance from Earth as a function of time. The maximum distance was ≃7 lt-s in 2002 January and May, when it was in a distant prograde orbit (DPO). Since 2004 *Wind* has been in a Lissajous orbit at the L_1 libration point of the Sun–Earth system at a distance of ≃5 lt-s.

(A color version of this figure is available in the online journal.)

For *Wind*, *INTEGRAL*, and near-Earth s/c, ephemeris uncertainties are negligible compared to uncertainties in time delays and we do not take them into account.

In total 356 *KW*–near-Earth s/c and *KW–INTEGRAL* annuli have been obtained. The histograms of Figure 5 show the distributions of uncertainties in time delays and 3σ HWs of these annuli. The smallest time delay uncertainty is 2 ms, the largest is 504 ms, the mean is 43 ms, and the geometrical mean is 23 ms. The smallest 3σ HW is 0.°027 (1.′6), the largest is 32.°2, the mean is 1.°30, and the geometrical mean is 0.°43.

In the following subsections some details on triangulation involving *KW*, *INTEGRAL*, and the near-Earth s/c are given.

4.2.1. KW–CGRO (BATSE) Triangulations

The BATSE was a high-energy astrophysics experiment aboard the *CGRO* (Fishman et al. 1992). Its Large Area Detectors measured burst time histories in four energy channels Ch1, Ch2, Ch3, Ch4, with approximate channel boundaries: 25–55 keV, 55–110 keV, 110–320 keV, and >320 keV. The clock on the *CGRO* is accurate to 100 μs, and this accuracy was verified through pulsar timing. Onboard software increases the uncertainty in the BATSE trigger times to ≃1 ms.

BATSE observed 52 *KW* short GRBs: 44 in the triggered mode, and 8 in the real-time mode. We derived *KW*-BATSE annuli for the 44 *KW* short bursts observed in the triggered mode and for 6 bursts observed by BATSE in real-time mode (these bursts were observed by only *KW* and BATSE).

For cross-correlation with triggered BATSE bursts we utilized *KW* light curves in the G2+G3 or in the G2 band with 2 or 16 ms resolution and BATSE concatenated light curves (DISCLA, PREB, and DISCSC data types) in the Ch2+Ch3+Ch4 or in the Ch2+Ch3 band with a time resolution of 64 ms. For several GRBs such light curves are not available and we utilized other types of BATSE data. Usually we tried different energy bands to check the consistency of the derived time delay and finally chose those with minimum χ^2. The cross-correlation curves for different bands may be slightly shifted relative each other (by several ms) but the 3σ intervals for cross-correlation lag τ are always in good agreement.

The resulting $\chi^2_{r,\min}$ range from 0.06 to 4.51 with a mean of 0.81. The maximum $\chi^2_{r,\min}$ of 4.51 (dof = 6) is a clear outlier in the distribution of bursts over $\chi^2_{r,\min}$. It corresponds to the exceptionally intense GRB19970704_T04097 (BATSE #6293) with a peak count rate of 1.8×10^5 counts s^{-1} (*KW* 2 ms time scale) and 6.9×10^5 counts s^{-1} (BATSE 64 ms time scale). Both light curves (*KW* and BATSE) must be significantly distorted due to dead-time and pile-up effects. The derived statistical uncertainty in the time delay is only 3 ms, so we added 6 ms systematic uncertainty to account for the distortions.

The derived uncertainties in the time delays range from 5 ms to 84 ms with a mean of 24 ms, and a geometrical mean of 18 ms. The resulting annuli 3σ HWs range from 0.°082 to 11.°0 with a mean of 1.°14, and a geometrical mean of 0.°60. The widest annulus with HW of 11.°0 was obtained for GRB19991001_T04950 (BATSE #7781)—at that time *Wind* was only 0.34 lt-s from Earth.

The distances between the center lines of the *KW*-BATSE annuli and the centers of BATSE locations range from 0.°007 to 7.°7 with a mean of 2.°23. For 14 bursts the BATSE error circle does not intersect the *KW*-BATSE annulus and the distances from the closest boundary of the annulus range from 1.02σ to 7.2σ.[33]

Of the 52 bursts, 16 were observed by only *KW* and BATSE, and 12 were observed by only *KW*, BATSE, and *BeppoSAX*. For these bursts, we constrained the burst location to a segment of

[33] For GRB19961225_T36436 (BATSE #5725) the BATSE position given in the current BATSE catalog (R.A., decl.(J2000), Err = 171.°31, −2.°85, 1.°5) is 25.°2 away from the center line of the 1.°6 wide *KW*-BATSE annulus. This GRB is a "mirror" case for BATSE, with a bimodal probability distribution for the location. The alternative solution is R.A., decl.(J2000) = 141.°4, −5.°5, with a statistical error of 1.°8 (M. Briggs 2011, private communication). This position is 7.°3 away from the center line of the *KW*-BATSE annulus. We use this alternative BATSE position here.

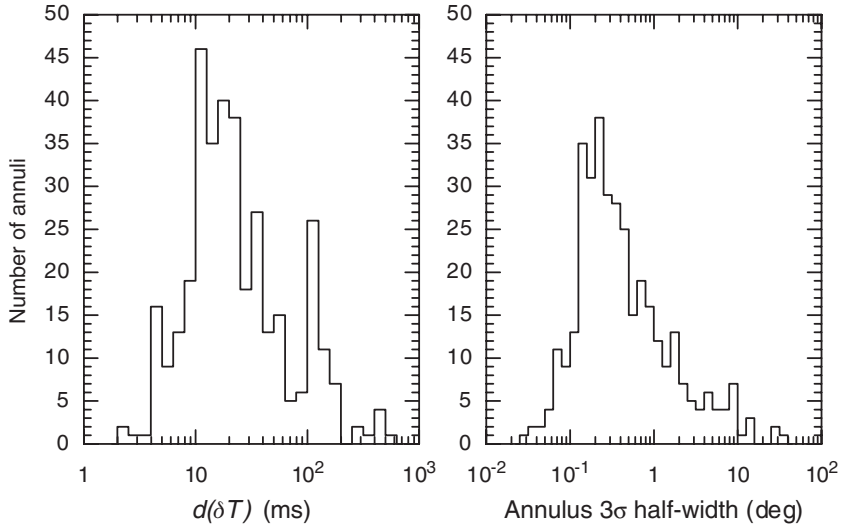

Figure 5. Distributions of uncertainties in time delay $d(\delta T) \equiv (d_+(\delta T) + |d_-(\delta T)|)/2$ and 3σ half-widths (HWs) of the 356 triangulation annuli obtained using the Konus-*Wind* and near-Earth (or *INTEGRAL*) s/c data. The smallest $d(\delta T)$ is 2 ms, the largest is 504 ms, the mean is 43 ms, and the geometrical mean is 23 ms. The smallest HW is $0\overset{\circ}{.}027$ ($1\overset{'}{.}6$), the largest is $32\overset{\circ}{.}2$, the mean is $1\overset{\circ}{.}30$, and the geometrical mean is $0\overset{\circ}{.}43$.

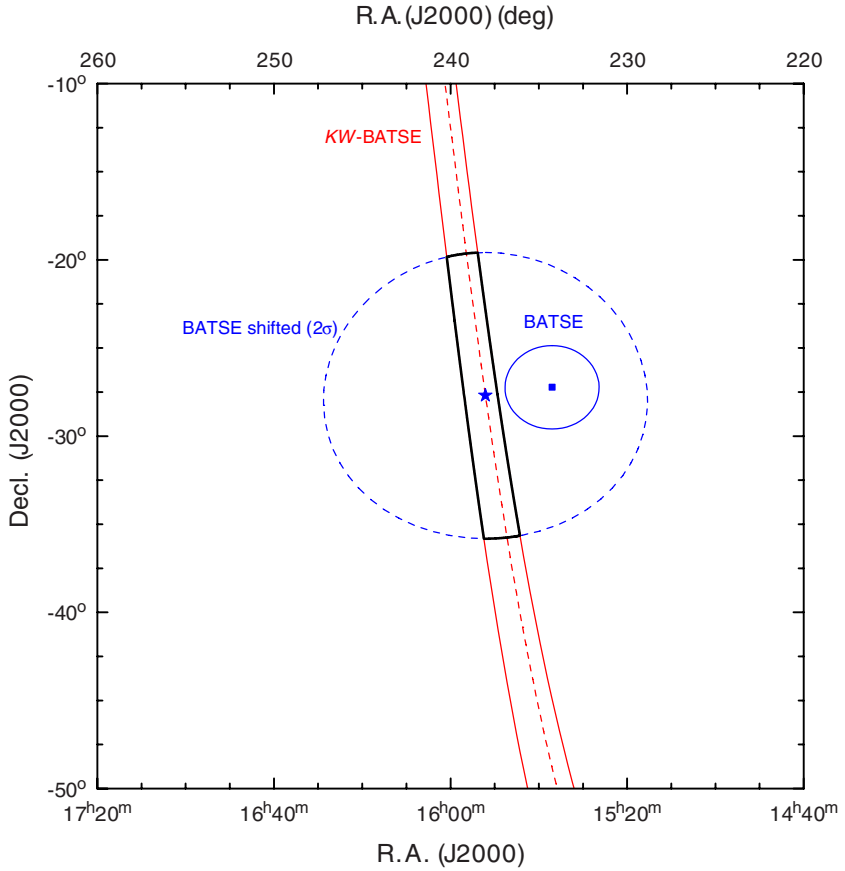

Figure 6. IPN/BATSE localization of GRB19960420_T16844 (BATSE #5439). The center of the BATSE error circle (R.A., decl.(J2000), Err = $234\overset{\circ}{.}25$, $-27\overset{\circ}{.}23$, $2\overset{\circ}{.}37$) lies $3\overset{\circ}{.}38$ from the center line of the $1\overset{\circ}{.}67$ wide *KW*-BATSE annulus. The resulting long box is shown by the solid black line and its center (that is, the nearest point to the BATSE center at the annulus center line) is indicated by the asterisk. The corners of the box are formed by the intersection of the circle centered at the asterisk with a radius of $8\overset{\circ}{.}12$, that is the sum of the 2σ BATSE error radius and $3\overset{\circ}{.}38$ systematics (dashed line), and the *KW*-BATSE annulus.

(A color version of this figure is available in the online journal.)

the *KW*-BATSE annulus using the following method. We took the center of the segment to be the point on the annulus center line nearest to the center of the BATSE position, and then we derived the corners of the segment from the intersection of the annulus and a circle centered at this point with a radius equal to the sum of twice the BATSE 1σ error and a systematic error, taken to be the larger of $2\overset{\circ}{.}0$ and the distance between the BATSE position and the center line of the annulus (a core systematic error of $\simeq 2^\circ$ was found for BATSE locations; see Briggs et al. 1999). This is illustrated in Figure 6.

4.2.2. KW–Fermi (GBM) Triangulations

The GBM on board the *Fermi* observatory is primarily designed to study of GRBs by making observations in the ~8 keV–40 MeV band (Meegan et al. 2009). The GBM has the advantage of high effective area and time-tagged data. The absolute timing of the GBM clock has an accuracy better than 20 μs. The GBM TTE data contain counts in 128 energy channels from ~5 keV to 2 MeV, which enables the preparation of the GBM light curve in three energy channels which are nearly the same as those of *KW*.

GBM observed 34 *KW* short GRBs. We derived *KW*-GBM triangulation annuli for all of them.

For cross-correlation we utilized *KW* light curves in the G2+G3 or in the G2 band with 2 or 16 ms resolution and GBM light curves with 1 or 16 ms resolution made from the TTE data (only NaI data were used).

The resulting $\chi^2_{r,\min}$ range from 0.16 to 2.10 with a mean of 0.90. The derived uncertainties in the time delays range from 2.5 ms to 136 ms with a mean of 22 ms, and a geometrical mean of 15 ms. The resulting annuli 3σ HWs range from $0\overset{\circ}{.}035$ ($2\overset{'}{.}1$) to $1\overset{\circ}{.}65$ with a mean of $0\overset{\circ}{.}35$, and a geometrical mean of $0\overset{\circ}{.}23$.

4.2.3. KW–INTEGRAL (SPI-ACS) Triangulations

The ACS of the SPI instrument on-board *INTEGRAL*, besides serving to veto the background in the germanium spectrometer, is routinely used as a nearly omnidirectional detector for GRBs (von Kienlin et al. 2003). It measures burst light curves with a time resolution of 50 ms in a single energy range above ~80 keV (for more details see Lichti et al. 2000). A systematic error in the ACS timing of 125 ± 10 ms has been found (Rau et al. 2004) and all SPI-ACS light curves have been corrected automatically for this error after 2004 April; corrections for it were applied by hand to the data prior to this date.

This systematic uncertainty is related to the approximate nature of conversion from on-board time to UTC used in producing SPI-ACS light curves in real time (within just seconds after the event at ftp://isdcarc.unige.ch/arc/FTP/ibas/spiacs/).

On the other hand, the time conversion used in archived and near real-time data is precise. Recently it was shown that the drift of the ACS clock with respect to the germanium detector clock during the whole *INTEGRAL* mission is around 1 ms (Zhang et al. 2010), thereby reducing the systematic uncertainty of ACS timing from 10 ms to 1 ms.

SPI-ACS light curves corrected for systematic shifts and characterized by high timing precision (at least down to 1 ms) are available in the *INTEGRAL* data archive since revision 3. The archived and equally precise near real-time data (available within hours after the observation) are accessible through Web services http://isdc.unige.ch/~savchenk/spiacs-online/ and http://www.isdc.unige.ch/heavens/. They are routinely used for near real-time triangulation.

SPI-ACS observed 139 *KW* short GRBs. We derived *KW*-SPI-ACS annuli for 103 of them.

For cross-correlation we utilized *KW* light curves in the G2+G3 or in the G3 band with 2 or 16 ms resolution.

The resulting $\chi^2_{r,\min}$ range from 0.04 to 3.96 with a mean of 1.02. The derived uncertainties in the time delays range from 4 ms to 175 ms with a mean of 24 ms, and a geometrical mean of 19 ms. The resulting annuli 3σ HWs range from $0\overset{\circ}{.}047$ ($2\overset{'}{.}8$) to $4\overset{\circ}{.}3$ with a mean of $0\overset{\circ}{.}41$, and a geometrical mean of $0\overset{\circ}{.}29$.

4.2.4. KW–Suzaku (WAM) Triangulations

The WAM is the active shield of the Hard X-ray detector on board the *Suzaku* mission (Yamaoka et al. 2009). In the triggered mode it measures light curves with a time resolution of 1/64 s in four energy channels which cover the ≃50–5000 keV range. In the real-time mode the time resolution is 1 s.

It was established that the *Suzaku*-WAM timing is consistent with negligible systematic uncertainties (Yamaoka et al. 2009).

WAM observed 61 *KW* short GRBs: 51 in the triggered mode and 10 in the real-time mode. We derived *KW*-WAM annuli for 45 triggered bursts.

For cross-correlation we utilized *KW* light curves in the G2+G3 or in the G3 band with 2 or 16 ms resolution and WAM light curves summed over four energy channels of 1 to 4 WAM detectors with the strongest response.

The resulting $\chi^2_{r,\min}$ range from 0.21 to 1.78 with a mean of 1.03. The derived uncertainties in the time delays range from 4 ms to 104 ms with a mean of 20 ms, and a geometrical mean of 14 ms. The resulting annuli 3σ HWs range from $0\overset{\circ}{.}060$ ($3\overset{'}{.}6$) to $2\overset{\circ}{.}44$ with a mean of $0\overset{\circ}{.}30$, and a geometrical mean of $0\overset{\circ}{.}21$.

4.2.5. KW–BeppoSAX (GRBM) Triangulations

The *BeppoSAX* GRBM was the anticoincidence shield of the high energy experiment Phoswich Detection System (Frontera et al. 1997; Feroci et al. 1997).

In the triggered mode it measured light curves with a time resolution of 7.8125 ms in the 40–700 keV range; in the real-time mode the time-resolution was 1 s (for more details see Frontera et al. 2009).

GRBM observed 50 *KW* short GRBs: 41 in the triggered mode and 9 in the real-time mode. We derived *KW*-GRBM annuli for 38 bursts observed in the triggered mode and for one burst observed in the real-time mode (this burst was observed by only *KW* and GRBM).

For cross-correlation we utilized *KW* light curves in the G2 or in the G2+G3 band with 2 or 16 ms resolution and GRBM light curves rebinned to 32 ms.

The resulting $\chi^2_{r,\min}$ range from 0.25 to 12.1 with a mean of 1.43. The maximum $\chi^2_{r,\min}$ of 12.1 (dof = 6) is a clear outlier in the distribution of bursts over $\chi^2_{r,\min}$. It corresponds to the exceptionally intense GRB19970704_T04097 with a peak count rate of 1.8×10^5 counts s^{-1} (*KW* 2 ms time scale) and 1.5×10^5 counts s^{-1} (GRBM 32 ms time scale). Both light curves (*KW* and GRBM) must be significantly distorted due to dead-time and pile-up effects. The derived statistical uncertainty in the time delay is only 2 ms, so we increased this uncertainty to 6 ms to account for the distortions.

The derived statistical uncertainties in the time delays range from 4.5 ms to 216 ms with a mean of 32 ms, and a geometrical mean of 18 ms.

Comparison of the initially derived annuli with other available IPN annuli as well as comparison of the GRBM and BATSE light curves for common bursts has revealed a systematic error in the GRBM timing up to 100 ms. Since this error varies from burst to burst (both in value and in sign), we had to introduce 100 ms systematic error for *KW–SAX* triangulations. This leads to a significant broadening of the annuli, so their final 3σ HWs range from $1\overset{\circ}{.}23$ to $32\overset{\circ}{.}2$ with a mean of $5\overset{\circ}{.}30$, and a geometrical mean of $3\overset{\circ}{.}87$.

4.2.6. KW–Swift (BAT) Triangulations

The *Swift* BAT is a highly sensitive, large field of view (FOV) coded aperture telescope that detects and localizes GRBs in real time (Barthelmy et al. 2005). When a burst occurs outside its FOV, it cannot be imaged, but the BAT light curve can be used for triangulation. For such bursts the 64 ms light curves in the four standard BAT energy channels (15–25 keV, 25–50 keV, 50–100 keV, and 100–350 keV) are always available. For some bursts, TTE data are available, enabling any desired energy and time binning.

BAT observed 44 *KW* short bursts outside its FOV. We derived *KW*-BAT annuli for 23 of them.

For cross-correlation we utilized *KW* light curves in the G2 or in the G2+G3 band with 2 or 16 ms resolution and BAT 64 ms light curves usually taken in the energy range above 50 keV (which often provides the best S/N and corresponds better to the *KW* energy band).

The resulting $\chi^2_{r,\min}$ range from 0.25 to 7.48 with a mean of 1.41. The maximum $\chi^2_{r,\min}$ of 7.48 (dof = 6) is a clear outlier in the distribution of bursts over $\chi^2_{r,\min}$. It corresponds to the exceptionally intense GRB20060306_T55358 with strong spectral evolution and a peak count rate of 1.9×10^5 counts s^{-1} (*KW* 2 ms time scale). The derived statistical uncertainty in the time delay is only 5 ms, so we added 10 ms systematic uncertainty.

The derived uncertainties in the time delays range from 5 ms to 64 ms with a mean of 22 ms, and a geometrical mean of 18 ms. The resulting annuli 3σ HWs range from $0\overset{\circ}{.}059$ ($3\overset{'}{.}5$) to $1\overset{\circ}{.}18$ with a mean of $0\overset{\circ}{.}41$, and a geometrical mean of $0\overset{\circ}{.}29$.

4.2.7. KW–Coronas-F (Helicon) Triangulations

The Helicon gamma-ray spectrometer was one of the instruments on board the *Coronas-F* solar space observatory (Oraevskii et al. 2002). It was similar to the *KW* spectrometer in the characteristics of its two detectors and in the data presentation structure. The similar design of both instruments enabled good cross-correlations of burst light curves.

Helicon observed 14 *KW* short GRBs. We derived *KW*-Helicon annuli for all of them.

The resulting $\chi^2_{r,\min}$ range from 0.25 to 2.67 with a mean of 1.02. The derived uncertainties in the time delays range from 4 ms to 80 ms with a mean of 25 ms, and a geometrical mean of 17 ms. The resulting annuli 3σ HWs range from $0\overset{\circ}{.}045$ ($2\overset{'}{.}7$) to $1\overset{\circ}{.}15$ with a mean of $0\overset{\circ}{.}38$, and a geometrical mean of $0\overset{\circ}{.}25$.

4.2.8. KW–Cosmos (Konus-A, A2, A3) Triangulations

Konus-A, Konus-A2, and Konus-A3 were gamma-ray spectrometers on board *Cosmos* spacecraft 2326, 2367, and 2421, respectively. A brief description of the Konus-A instrument is given in Aptekar et al. (1998). Konus-A2 and Konus-A3 were similar to Konus-A in the characteristics of its detectors and in the data presentation structure.

They observed five *KW* short GRBs in the triggered mode. We derived *KW-KA* annuli for four of them.

The resulting $\chi^2_{r,\min}$ range from 0.73 to 1.42 with a mean of 1.07. The derived uncertainties in the time delays range from 4 ms to 56 ms with a mean of 35 ms. The resulting annuli 3σ HWs range from $0\overset{\circ}{.}15$ to $1\overset{\circ}{.}20$ with a mean of $0\overset{\circ}{.}79$.

4.2.9. KW–RHESSI Triangulations

The *RHESSI* is a high resolution spectrometer designed to study high-energy emission from solar flares over a broad energy range from 3 keV to 17 MeV (Lin et al. 2002; Smith et al. 2002). The data are collected in the TTE mode enabling arbitrary energy and time binning.

RHESSI observed 58 *KW* short GRBs. We derived *KW-RHESSI* annuli for 32 bursts.

For cross-correlation we utilized *KW* light curve in the G2, in the G1+G2, or in the G2+G3 band with 2, 16, 64, and 256-ms resolution (depending on burst intensity).

The resulting $\chi^2_{r,\min}$ range from 0.36 to 2.62 with a mean of 1.07. The derived uncertainties in the time delays range from 2 ms to 184 ms with a mean of 36 ms, and a geometrical mean of 20 ms. The resulting annuli 3σ HWs range from $0\overset{\circ}{.}027$ ($1\overset{'}{.}6$) to $2\overset{\circ}{.}71$ with a mean of $0\overset{\circ}{.}53$, and a geometrical mean of $0\overset{\circ}{.}30$.

4.2.10. KW–HETE-2 (FREGATE) Triangulations

The gamma-ray detector of *HETE-2*, called FREGATE, was designed to detect GRBs in the energy range 8–400 keV (Ricker et al. 2003; Atteia et al. 2003).

In the triggered mode it measures light curves with a time resolution of 1/32 s in the 8–400 keV range; in the real-time mode the time-resolution is 0.1638 s.

FREGATE observed 16 *KW* short GRBs: 8 in the triggered mode and 8 in the real-time mode. In most cases the FREGATE response is significantly weaker than the responses of other instruments flying on low-Earth s/c, so we used the FREGATE data only for a few cases when no other low-Earth s/c detected the burst. We derived *KW–HETE* annuli for four bursts observed in the triggered mode.

For cross-correlation we utilized *KW* light curve in the G2 or in the G2+G3 band with 2 or 16 ms resolution.

The resulting $\chi^2_{r,\min}$ range from 0.50 to 1.43 with a mean of 0.96. The derived uncertainties in the time delays range from 56 ms to 168 ms with a mean of 102 ms. The resulting annuli 3σ HWs range from $0\overset{\circ}{.}95$ to $1\overset{\circ}{.}47$ with a mean of $1\overset{\circ}{.}10$.

4.2.11. KW–AGILE (MCAL) Triangulations

The MCAL on board the *AGILE* mission is a spectrometer sensitive to gamma-rays in the energy band $\simeq$0.35–100 MeV (Tavani et al. 2009). MCAL has the advantage of time-tagged data.

MCAL observed 24 *KW* short GRBs: 22 in the triggered mode and 2 in the real-time mode. In many cases the MCAL response is rather weak due to its high energy threshold and strong attenuation by the GRID instrument, so we used the MCAL data only for several intense bursts. In total we derived nine *KW*-MCAL annuli.

For cross-correlation we utilized *KW* light curve in the G3 or in the G2+G3 band with 2 or 16 ms resolution.

The resulting $\chi^2_{r,\min}$ range from 0.29 to 2.26 with a mean of 1.08. The derived uncertainties in the time delays range from 5 ms to 21 ms with a mean of 13 ms. The resulting annuli 3σ HWs range from $0\overset{\circ}{.}071$ ($4\overset{'}{.}3$) to $0\overset{\circ}{.}60$ with a mean of $0\overset{\circ}{.}21$.

4.2.12. INTEGRAL–near-Earth s/c Triangulations

Even without the planetary missions, the mini-network of low-Earth orbiters, plus *INTEGRAL* and Konus-*Wind*, often make it possible to obtain error boxes for many bursts. Since *INTEGRAL* orbits at distances $\lesssim$0.5 lt-s, which are much smaller than the *Wind*-to-Earth distance $\simeq$5 lt-s, *KW–INTEGRAL* and *KW*–near-Earth s/c annuli intersect at grazing incidence, resulting in one or two long boxes. In some cases, the intersection of *KW*–near-Earth s/c and *INTEGRAL*–near-Earth s/c results in smaller localization regions.

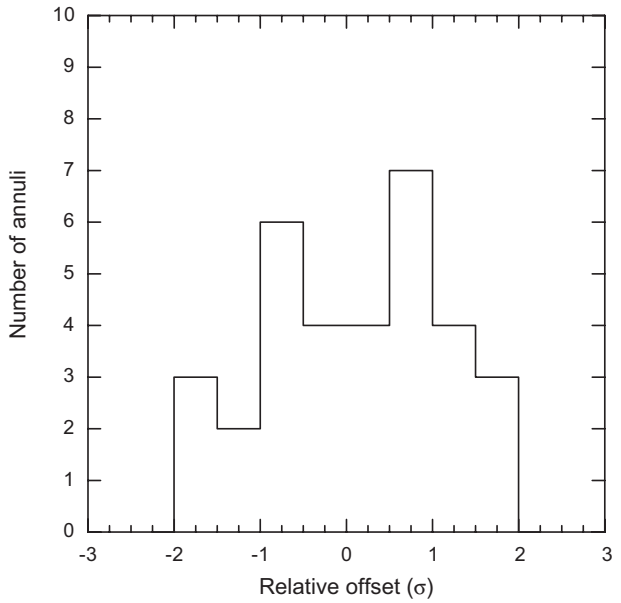

Figure 7. Distribution of the offsets of the accurate GRB positions from the center lines of the 33 *KW*–near-Earth (or *INTEGRAL*) s/c annuli.

In total 11 *INTEGRAL*–near-Earth s/c annuli have been obtained. The resulting annuli HWs range from 1.°0 to 14.°0 with a mean of 5.°9.

4.3. Verifying Triangulation Annuli

Of the 271 Konus short bursts localized by IPN, 17 were precisely localized by instruments with imaging capabilities: 15 by *Swift*-BAT (one of them, GRB 090510, was also localized by *Fermi*-LAT), 1 by *HETE-2* (WXM and SXC), and 1 by *INTEGRAL* IBIS/ISGRI.

We utilized these bursts to verify our triangulations. For these 17 bursts, 21 *KW*–near-Earth s/c, and 12 *KW–INTEGRAL* annuli were obtained (we have not used the light curves of the instruments which imaged the burst, since the instrument response for imaged bursts is different from those detected outside the FOV and used for IPN triangulations). In each case the triangulation annuli are in agreement with the known position of the source, thereby confirming the reliability of our triangulations. Indeed, such tests constitute "end-to-end" calibrations, as they confirm not only spacecraft timing and ephemeris information, but also the cross-correlations of the various time histories and derivations of the annuli.

The histograms of Figure 7 show the distribution of relative source offsets from the center lines of the annuli. One can see that all offsets (in absolute values) are less than 2σ. The minimum offset of the precise position is -2.0σ, the maximum is 1.9σ, the average is 0.04σ, and the standard deviation is 1.1σ.

Besides this verification, the consistency of several *KW*–near-Earth s/c annuli often obtained for a given burst with each other and with distant s/c annuli (when available) confirms the reliability of our *KW*–near-Earth triangulations, many of which have time delay uncertainties less than 10–20 ms (see Figure 5).

5. LOCALIZATIONS: ADDITIONAL CONSTRAINS

In addition to triangulation annuli, several other types of localization information are included in this catalog. They are ecliptic latitude range, autonomous burst localizations obtained by *CGRO* BATSE, *BeppoSAX* GRBM, and *Fermi* GBM, and Earth- or Mars-blocking (*MESSENGER* is in an eccentric orbit around Mercury, so Mercury-blocking is quite rare). This additional information helps constrain the triangulation position, i.e., to choose one of two triangulation boxes, or to eliminate portions of a single annulus.

5.1. Ecliptic Latitudes

The ecliptic latitudes of the bursts are derived by comparing the count rates of the two *KW* detectors taken in the waiting mode with 1.472 s or 2.944 s time resolution. The axis of the detector S2 points towards the north ecliptic pole, and the axis of S1 points toward the south ecliptic pole. In addition to statistical uncertainties, the ecliptic latitude determination is subject to systematic uncertainties due to, among other things, time-variable cosmic X-ray sources and absorption by other instruments aboard the spin-stabilized *Wind* spacecraft. The estimated ecliptic latitudes can be taken to be at the 95% confidence level.

The ecliptic latitude range, namely the best estimate of b, and the lower and upper limits $b_{\rm min}$, $b_{\rm max}$ can be considered to be an annulus centered at the north or south ecliptic pole, with a half-angle $\theta = 90^\circ - |b|$ and HWs $d_-(\theta) = b_{\rm min} - b$, $d_+(\theta) = b_{\rm max} - b$.

5.2. Planet Blocking

Planet blocking is specified by the right ascension and declination of the planet's center and its radius. When a spacecraft in low Earth or Mars orbit observes a burst, the planet blocks up to ≈3.7 sr of the sky. The source position must be outside this occulted part of the sky.

The allowed part of the sky can be described as a degenerate annulus centered at the direction opposite to the planet's center, with a half-angle $\theta = 0$ whose widths $d_-(\theta) = 0$, $d_+(\theta) = \sin^{-1}(R_{\rm planet}/R)$, where R is the radius of the s/c orbit (here we neglect the oblateness of the planet and absorption in its atmosphere).

5.3. Autonomous Localizations

A principle of autonomous burst localization using a system of detectors possessing anisotropic angular sensitivity was suggested by Golenetskii et al. (1974) and first implemented in the Konus instruments on the *Venera 11* and *12* missions (Mazets & Golenetskii 1981).

Similar localization systems consisting of different numbers of detectors have been placed on *CGRO* (BATSE), *BeppoSAX* (GRBM), and *Fermi* (GBM). These autonomous localizations, derived by comparing the count rates of various detectors, are affected by Earth albedo and absorption by spacecraft materials, among other things, and their shapes are in general complex. The error circles are approximations to these shapes. They are centered at the point which is the most likely arrival direction for the burst, and their radii are defined so that their areas are equal to the 1σ(BATSE, GBM) or 90% confidence (GRBM) statistical-only true error regions. All these localizations also have systematic errors of several degrees or more.

These error circles can also be described as degenerate annuli centered at the most likely arrival direction for the burst, with a half-angle $\theta = 0$ whose widths $d_-(\theta) = 0$, $d_+(\theta) = r$, where r is the positional error.

6. LOCALIZATIONS: RESULTS

Table 2 summarizes localization information for 271 Konus short bursts. The first column gives the burst designation (see

Table 2
IPN Localization Data

Designation	N	Location[a] Source	R.A. (J2000) (deg)	Decl. (J2000) (deg)	θ (deg)	$d_-(\theta)$ (deg)	$d_+(\theta)$ (deg)
GRB19950210_T08424	4	Uly-GRO	155.4443	+25.7475	53.6317	−0.0078	+0.0078
		KW-GRO	130.3580	+18.8483	52.3229	−0.1532	+0.1189
		Ecl.Band	90.000	−66.561	43.3	−19.5	+46.0
		BATSE	154.55	−27.48	0	0	1.15
GRB19950211_T08697	4	Uly-GRO	335.8036	−25.1240	85.8298	−0.0063	+0.0063
		KW-GRO	311.5868	−18.2357	89.9796	−0.0678	+0.1221
		Ecl.Band	270.000	66.561	65.5	−39.5	+22.6
		BATSE	9.51	52.65	0	0	1.08

Notes. [a] sc_1-sc_2—IPN annulus obtained using sc_1 and sc_2 data; Ecl.Band—the ecliptic latitude band of the burst; sc—spacecraft/instrument which imaged or autonomously localized the burst; Occ.sc—the occulted part of the sky for sc. The s/c name abbreviations are given in Table 1. For autonomous localizations the instrument names are given (i.e., BATSE, GRBM, GBM). BATSEbg—localization from the BATSE untriggered burst catalog (Stern et al. 2001). BATSEshift—BATSE localization modified as described in Section 4.2.1.

(This table is available in its entirety in a machine-readable form in the online journal. A portion is shown here for guidance regarding its form and content.)

Table 1). The second column gives the number of localization constraints (the number of rows with localization information for the burst). The six subsequent columns give localizations expressed as a set of annuli: the third column gives the source of the location: either sc1–sc2 (triangulation annulus derived using sc1 and sc2), or "Ecl.Band" (range of ecliptic latitudes), or "Instr" (name of the instrument which autonomously localized the bursts), or "Occ.sc" (planet blocking); Columns 4–8 list the right ascension and declination of the annulus center (J2000), the annulus radius θ, and the 3σ uncertainties in the radius $d_-(\theta)$, $d_+(\theta)$.

Planet blocking is given only if it constrains the location. The ecliptic latitude range is given for all bursts. All available autonomous localizations are given.

The *Swift*-BAT localizations are taken from the second *Swift* BAT catalog covering 2004 December 19 to 2009 December 21 (Sakamoto et al. 2011), and for the latest bursts from the GCN Circulars with BAT refined positions.

The *HETE-2* localizations for GRB 040924 (=GRB20040924_T42735) is taken from Arimoto et al. (2006).

The IBIS/ISGRI localization for GRB 070707 (=GRB20070707_T58122) is taken from Götz et al. (2007).

The BATSE localizations are taken from the current catalog on the BATSE Web site,[34] as well as from the BATSE untriggered burst catalogs (Stern et al. 2001; Kommers et al. 2000).[35]

The *BeppoSAX* localizations are taken either from the GRBM catalog (Frontera et al. 2009) or from the IAU and GCN Circulars.

The GBM localizations are taken from the first *Fermi* GBM catalog covering 2008 July 12 to 2010 July 11 (Paciesas et al. 2012), the GCN Circulars, or from the latest version of the corresponding "glg_tcat*.fit" file in the GBM data archive.[36]

6.1. Boxes

For those bursts which were detected by three or more well separated s/c, a triangulation box can be derived.

In general, the intersection of two annuli involving distant s/c gives a small box with an area as small as 1 arcmin^2.

The intersection of two annuli derived from a distant s/c, Konus-*Wind*, and a near-Earth s/c usually gives an elongated box, which nevertheless in most cases has a small area of several hundred arcmin^2. In some cases the intersection of annuli derived from a single distant s/c, Konus-*Wind*, and a near-Earth s/c can give a smaller error box than annuli derived using two distant s/c.

Long boxes were derived for bursts not observed by any distant s/c, but observed by *KW*, *INTEGRAL* SPI-ACS, and one or more near-Earth s/c. In such cases, the box is formed by a *KW*–near-Earth s/c annulus and an *INTEGRAL*–near-Earth s/c annulus, or by a *KW*–near-Earth s/c annulus and a *KW–INTEGRAL* annulus intersecting at grazing incidence.

In all cases, if the three s/c which formed the box were nearly aligned, the annuli intersect at grazing incidence, resulting in a long box.

In total we derived 162 error boxes for Konus short bursts: 27 for bursts observed by two distant s/c, 84 for bursts observed by one distant s/c and at least one near-Earth s/c, and 51 for bursts observed by only *KW*, *INTEGRAL*, and one or more near-Earth s/c. In some cases these error regions are actually long arcs rather than boxes (in particular this is a case when the burst was not observed by a distant s/c), but for simplicity we still refer to them as boxes since they are formed by intersection of two or more triangulation annuli.

6.2. Segments

For those bursts which were detected only by *KW* and another s/c, or by *KW* and one or more near-Earth s/c, the resulting localization is formed by a triangulation annulus (the narrowest in the case of several *KW*–near-Earth s/c annuli) and additional constraints. These localizations consist of the entire annulus (in the case where it is entirely inside the allowed ecliptic latitude band and there are no other constraints) or one or two annulus segments, formed by the intersection of the annulus with the ecliptic latitude band, and/or by exclusion of the occulted part of the annulus, or by combination with the BATSE localization (see Section 4.2.1).

One hundred and fourteen bursts had this kind of localization: 20 were bursts observed by *KW* and a distant s/c (of these, 3 were also observed by a near-Earth s/c in real-time mode, but

[34] http://www.batse.msfc.nasa.gov/batse/grb/catalog/current/

[35] Since the catalog by Stern et al. (2001) contains the localizations for all eight Konus short bursts detected by BATSE in the real-time mode, and the catalog by Kommers et al. (2000) misses some of them, the given localizations are solely from Stern et al. (2001).

[36] ftp://legacy.gsfc.nasa.gov/fermi/data/gbm/bursts

Table 3
IPN Error Regions

Designation	N_r	N_c	Type[a]	Max. Dim. (deg)	Area (deg^2)	Formed by[b]	R.A. (J2000)[c] (deg)	Decl. (J2000)[c] (deg)
GRB19950210_T08424	1	4	B	5.65E-001	8.39E-003	Uly-GRO,KW-GRO,Ecl.Band	154.6820	−27.8792
							154.3544	−27.8662
							154.9633	−27.8744
							154.9330	−27.8897
							154.3240	−27.8812
GRB19950211_T08697	1	4	B	5.13E-001	6.09E-003	Uly-GRO,KW-GRO,Ecl.Band	14.7526	+53.8367
							14.5265	+53.9214
							15.1974	+53.6449
							15.1690	+53.6722
							14.4975	+53.9485

Notes.
[a] Type of the error region: B—box, LB—long box: maximum dimension >10°, S—annulus segment, and A—entire annulus.
[b] The localization data from Table 2 used to form the region(s).
[c] For localizations which are an entire annulus, these fields are empty (and only one row for the burst is given). The parameters of the annuli can be found in Table 2.
(This table is available in its entirety in a machine-readable form in the online journal. A portion is shown here for guidance regarding its form and content.)

KW–near-Earth s/c annuli have not been derived for them), and 94 were bursts observed by only *KW* and one or more near-Earth s/c.

6.3. Resulting Error Regions

Table 3 gives the description of the final IPN error regions for 254 Konus short bursts (this sample does not include the 17 imaged bursts). The nine columns contain the following information: (1) the burst designation (see Table 1), (2) the number of error regions for the burst, N_r: 1 or 2, (3) the number of corners of the region, N_c, (4) the region type: "B" (box), "LB" (long box: box with maximum dimension >10°), "S" (segment), or "A" (annulus), (5) the area (for two regions the sum of their areas), (6) the maximum dimension of the region (that is the maximum angular distance between two points at the region boundary; for segments larger than half an annulus, this is just the outer diameter of the annulus), (7) the right ascension of the center of the error region, in the first row, and the right ascensions of the corners in the following N_c rows, and (8) the declination of the center of the error region, in the first row, and the declinations of the corners in the following N_c rows (if there are two error regions, additional N_c+1 rows are given: the center of the second region and its corners, so the total number of rows for such a burst is 2(N_c+1)). All coordinates are J2000.

In general, a simple, four-corner error region description is inaccurate and the curvature of the annuli should be taken into account. Only in cases where the maximum dimension of the error region is less than several degrees, can the box be reasonably well represented by its four corners. In other cases, especially when the region is a long arc or annulus segment, the given corners and center are intended to roughly indicate the position of the region on the sky. Figures showing the IPN localization (all derived annuli and the resulting error region(s)) can be found at the Ioffe Web site.[37]

A histogram of IPN error region areas is shown in Figure 8. For bursts observed by distant s/c the areas range from 2.40 × 10^{-4} deg^2 (0.86 arcmin^2) to 142.1 deg^2 with a mean of 3.49 deg^2, and a geometrical mean of 0.141 deg^2. For bursts without distant s/c detections the areas range from 0.210 deg^2 to 4420 deg^2 with a mean of 242 deg^2, and a geometrical mean of 46.2 deg^2.

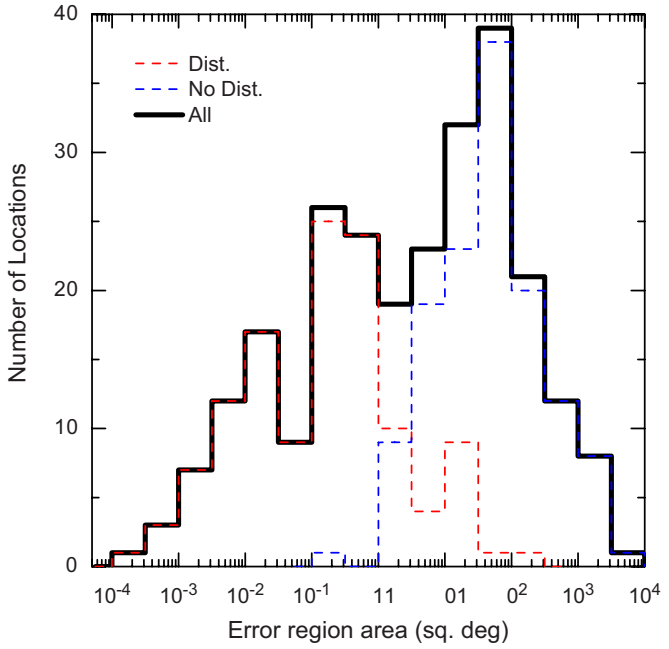

Figure 8. Distributions of error region areas for 123 Konus short bursts observed by at least one distant s/c (red dashed line), 131 bursts not observed by any distant s/c (blue dashed line), and all 254 bursts (17 imaged bursts are not counted).
(A color version of this figure is available in the online journal.)

7. COMMENTS ON SPECIFIC EVENTS

GRB 051103 (=GRB20051103_T33943) may in fact be a giant SGR flare in the nearby M81 group of interacting galaxies as was suggested by Frederiks et al. (2007). The final IPN localization of this event along with further exploration of this possibility are given in Hurley et al. (2010b). See also Ofek et al. (2006) for implications of the optical and radio followup observations and Abadie et al. (2012) for implications of the gravitational-wave non-detection of this event.

[37] http://www.ioffe.ru/LEA/ShortGRBs_IPN/

Table 4
Recent IPN Catalogs of Gamma-Ray Bursts

Years Covered	Number of GRBs	Description
1990–1992	16	*Ulysses, Pioneer Venus Orbiter,* WATCH, SIGMA, PHEBUS GRBs[a]
1990–1994	56	*Granat*-WATCH supplement[b]
1991–1992	37	*Pioneer Venus Orbiter, Compton Gamma-Ray Observatory, Ulysses* GRBs[c]
1991–1994	218	BATSE 3B supplement[d]
1991–2000	211	BATSE untriggered burst supplement[e]
1992–1993	9	*Mars Observer* GRBs[f]
1994–1996	147	BATSE 4Br supplement[g]
1994–2010	279	Konus short bursts[h]
1996–2000	343	BATSE 5B supplement[i]
1996–2002	475	*BeppoSAX* supplement[j]
2000–2006	226	*HETE-2* supplement[k]
2008–2010	146	GBM supplement[l]

Notes.
[a] Hurley et al. (2000a); [b] Hurley et al. (2000b); [c] Laros et al. (1998); [d] Hurley et al. (1999a); [e] Hurley et al. (2005); [f] Laros et al. (1997); [g] Hurley et al. (1999b); [h] Present catalog; [i] Hurley et al. (2011b); [j] Hurley et al. (2010a); [k] Hurley et al. (2011a); [l] Hurley et al. (2013).

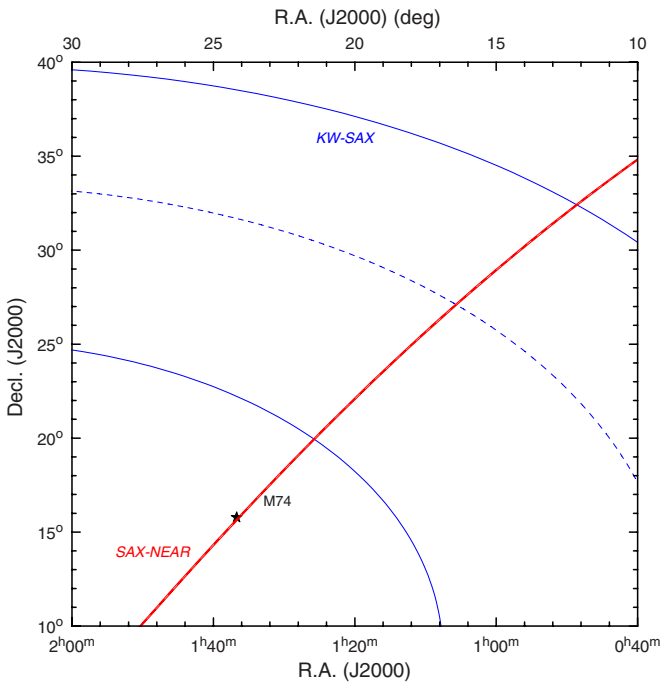

Figure 9. IPN localization of GRB 000420 (=GRB20000420_T42714). The 1.′7 wide *SAX–NEAR* annulus passes through the nearby M74 galaxy, while the galaxy is well outside the wide 3σ *KW–SAX* annulus.

(A color version of this figure is available in the online journal.)

GRB 070201 (=GRB20070201_T55390) is likely a giant SGR flare from the Andromeda galaxy (Mazets et al. 2008). See also Abbott et al. (2008) for implications of the gravitational-wave non-detection of this event, and Ofek et al. (2008) for implications of the optical afterglow and X-ray periodic source non-detections.

GRB 000420 (=GRB20000420_T42271): based on the *KW–NEAR* annulus it was suggested by Ofek (2007) that this burst might be associated with the nearby Sc-type galaxy M74 (NGC 628). The position of this galaxy lies well outside the wide *KW–SAX* annulus, thereby excluding it as a possible host for this short GRB—see Figure 9.

GRB 990405 (=GRB19990405_T30059): initially this event was classified as a burst from SGR 1900+14 since the narrow *SAX–Ulysses* annulus (3σ HW of 0.°035) passes through the position of this SGR. The derived wide *KW–SAX* annulus (3σ HW of 6.°4) is also consistent with the SGR position. But this burst is substantially harder than two unusually hard bursts from SGR 1900+14: 981022, 991001 (Woods et al. 1999), making the possible association of this burst with the SGR doubtful.

8. SUMMARY AND CONCLUSION

This paper continues a series of catalogs of GRB localizations obtained by arrival-time analysis, or "triangulation" between the spacecraft in the third IPN, as summarized in Table 4.

We have presented the most comprehensive IPN localization data on 271 Konus-*Wind* short bursts. For 254 bursts IPN error regions were obtained and for 17 bursts precisely localized by instruments with imaging capability IPN triangulation annuli were derived for calibration purposes.

In total we derived 517 triangulation annuli, including 150 annuli with distant s/c.

It was shown that for many shorts bursts *KW*–near-Earth s/c (or *INTEGRAL*) triangulation yields a rather narrow annulus (with HW sometimes comparable to or even better than the annuli using distant s/c data), thereby providing small error boxes with areas of several hundred arcmin^2 even for those *KW* short bursts which were detected by only one distant s/c (and one or more near-Earth s/c), and providing a long box in cases where the burst was detected by Konus-*Wind*, *INTEGRAL* SPI-ACS, and one or more near-Earth s/c.

The localizations can be used for a wide variety of purposes, including, but not limited to, searches for (1) gravitational wave and neutrino signals from merging compact objects (2) very high energy photons from the burst sources (3) giant SGR flares in nearby galaxies.

The Konus-*Wind* experiment is supported by a Russian Space Agency contract and RFBR grants 12-02-00032a and 13-02-12017-ofi-m. K.H. is grateful for IPN support under the following NASA, JPL, and MIT grants and contracts. JPL 958056 and 1268385 (*Ulysses*); NNX07AH52G and NNX12AE41G (ADA and ADAP); NAG5-12614, NNG04GM50G, NNG06GE69G, NNX07AQ22G, NNX08AC90G, NNX08AX95G and NNX09AR28G (*INTEGRAL*); NNG05GTF72G, NNG06GI89G, NNX07AJ65G,

NNX08AN23G, NNX09AO97G, NNX10AI23G, and NNX12AD68G (*Swift*); NAG5-3500 and NAG5-9503 (*NEAR*); MIT-SC-R-293291 and NAG5-11451 (*HETE-2*); JPL 1282043 (*Odyssey*); NNX06AI36G, NNX08AB84G, NNX08AZ85G, NNX09AV61G, NNX10AR12G (*Suzaku*); NNX09AU03G, NNX10AU34G, and NNX11AP96G (*Fermi*); NNX07AR71G (*MESSENGER*); NAG5-7766, NAG5-9126, and NAG5-10710 (*BeppoSAX*).

REFERENCES

Abadie, J., Abbott, B. P., Abbott, T. D., et al. 2012, ApJ, 755, 2
Abbott, B., Abbott, R., Adhikari, R., et al. 2008, ApJ, 681, 1419
Arimoto, M., Ricker, G., Atteia, J-L., et al. 2006, GCN, 4550
Aptekar, R., Frederiks, D., Golenetskii, S., et al. 1995, SSRv, 71, 265
Aptekar, R. L., Butterworth, P. S., Cline, T. L., et al. 1998, ApJ, 493, 404
Atteia, J.-L., Boer, M., Cotin, F., et al. 2003, in AIP Conf. Proc. 662, Gamma-Ray Burst and Afterglow Astronomy 2001, A Workshop Celebrating the First Year of the HETE Mission, ed. G. Ricker & R. Vanderspek (New York: AIP), 17
Barthelmy, S. D., Barbier, L. M., Cummings, J. R., et al. 2005, SSRv, 120, 143
Boynton, W. V., Feldman, W. C., Mitrofanov, I. G., et al. 2004, SSRv, 110, 37
Briggs, M. S., Pendleton, G. N., Kippen, R. M., et al. 1999, ApJS, 122, 503
Feroci, M., Frontera, F., Costa, E., et al. 1997, Proc. SPIE, 3114, 186
Fishman, G., Meegan, C., Wilson, R., Paciesas, W., & Pendleton, G. 1992, in Proc. Compton Observatory Science Workshop, ed. C. Shrader, N. Gehrels, & B. Dennis (NASA CP 3137; Greenbelt, MD: GSFC), 26
Frederiks, D. D., Palshin, V. D., Aptekar, R. L., et al. 2007, AstL, 33, 19
Frontera, F., Costa, E., dal Fiume, D., et al. 1997, A&AS, 122, 357
Frontera, F., Guidorzi, C., Montanari, E., et al. 2009, ApJS, 180, 192
Gehrels, N., Chincarini, G., Giommi, P., et al. 2004, ApJ, 611, 1005
Gold, R., Solomon, S., McNutt, R., et al. 2001, P&SS, 49, 1467
Goldsten, J. O., Rhodes, E. A., Boynton, W. V., et al. 2007, SSRv, 131, 339
Golenetskii, S. V., Il'Inskii, V. N., & Mazets, E. P. 1974, CosRe, 12, 706
Götz, D., Beckmann, V., Mereghetti, S., & Paizis, A. 2007, GCN, 6608
Hurley, K., Atteia, J.-L., Barraud, C., et al. 2011a, ApJS, 197, 34
Hurley, K., Briggs, M., Kippen, R. M., et al. 1999a, ApJS, 120, 399
Hurley, K., Briggs, M., Kippen, R. M., et al. 1999b, ApJS, 122, 497
Hurley, K., Briggs, M., Kippen, R. M., et al. 2011b, ApJS, 196, 1
Hurley, K., Guidorzi, C., Frontera, F., et al. 2010a, ApJS, 191, 179
Hurley, K., Laros, J., Brandt, S., et al. 2000a, ApJ, 533, 884
Hurley, K., Lund, N., Brandt, S., et al. 2000b, ApJS, 128, 549
Hurley, K., Mitrofanov, I., Kozyrev, A., et al. 2006, ApJS, 164, 124
Hurley, K., Pal'shin, V., Aptekar, R., et al. 2013, ApJS, 207, 39
Hurley, K., Rowlinson, A., Bellm, E., et al. 2010b, MNRAS, 403, 342
Hurley, K., Sommer, M., Atteia, J.-L., et al. 1992, A&AS, 92, 401
Hurley, K., Stern, B., Kommers, J., et al. 2005, ApJS, 156, 217
Kommers, J., Lewin, W., Kouveliotou, C., et al. 2000, ApJ, 533, 696
Laros, J., Boynton, W., Hurley, K., et al. 1997, ApJS, 110, 157
Laros, J., Hurley, K., Fenimore, E., et al. 1998, ApJS, 118, 391
Lichti, G. G., Georgii, R., von Kienlin, A., et al. 2000, in AIP Conf. Proc. 510, The Fifth Compton Symposium, ed. M. L. McConnell & J. M. Ryan (New York: AIP), 722
Lin, R. P., Dennis, B. R., Hurford, G. J., et al. 2002, SoPh, 210, 3
Marar, T. M. K., Sharma, M. R., Seetha, S., et al. 1994, A&A, 283, 698
Mazets, E. P., Aptekar, R. L., Cline, T. L., et al. 2008, ApJ, 680, 545
Mazets, E. P., & Golenetskii, S. V. 1981, Ap&SS, 75, 47
Meegan, C., Lichti, G., Bhat, P. N., et al. 2009, ApJ, 702, 791
Norris, J. P., Scargle, J. D., & Bonnell, J. T. 2001, in Gamma-Ray Bursts in the Afterglow Era, ed. E. Costa, F. Frontera, & J. Hjorth (Berlin: Springer), 40
Ofek, E. O. 2007, ApJ, 659, 339
Ofek, E. O., Kulkarni, S. R., Nakar, E., et al. 2006, ApJ, 652, 507
Ofek, E. O., Muno, M., Quimby, R., et al. 2008, ApJ, 681, 1464
Oraevskii, V. N., Sobelman, I. I., Zhitnik, I. A., & Kuznetsov, V. D. 2002, PhyU, 45, 886
Paciesas, W. S., Meegan, C., von Kienlin, A., et al. 2012, ApJS, 199, 18
Rau, A., von Kienlin, A., Hurley, K., & Lichti, G. 2005, A&A, 438, 1175
Rau, A., von Kienlin, A., Lichti, G., Hurley, K., & Beck, M. 2004, GCN, 2568
Ricker, G. R., Atteia, J.-L., Crew, G. B., et al. 2003, in AIP Conf. Proc. 662, Gamma-Ray Burst and Afterglow Astronomy 2001, A Workshop Celebrating the First Year of the HETE Mission, ed. G. Ricker & R. Vanderspek (New York: AIP), 3
Sakamoto, T., Barthelmy, S. D., Baumgartner, W. H., et al. 2011, ApJS, 195, 2
Saunders, R. S., Arvidson, R. E., Badhwar, G. D, et al. 2004, SSRv, 110, 1
Smith, D. M., Lin, R., Turin, P., et al. 2002, SoPh, 210, 33
Solomon, S. C., McNutt, R. L., Gold, R. E., & Domingue, D. L. 2007, SSRv, 131, 3
Stern, B., Tikhomirova, Y., Kompaneets, D., Svensson, R., & Poutanen, J. 2001, ApJ, 563, 80
Takahashi, T., Abe, K., Endo, M., et al. 2007, PASJ, 59, S35
Tavani, M., Barbiellini, G., Argan, A., et al. 2009, A&A, 502, 995
Terrell, J., & Klebesadel, R. 2004, in AIP Conf. Proc. 727, Gamma-Ray Bursts: 30 Years of Discovery, ed. E. Fenimore & M. Galassi (New York: AIP), 541
Terrell, J., Lee, P., Klebesadel, R., & Griffee, 1996, in AIP Conf. Proc. 384, 3rd Huntsville Symposium, ed. C. Kouveliotou, M. Briggs, & G. Fishman (New York: AIP), 545
Terrell, J., Lee, P., Klebesadel, R., & Griffee, J. 1998, in AIP Conf. Proc. 428, Gamma-Ray Bursts, 4th Huntsville Symposium, ed. C. Meegan, R. Preece, & T. Koshut (New York: AIP), 54
Trombka, J. I., Boynton, W. V., Brückner, J., et al. 1999, NIMPA, 422, 572
von Kienlin, A., Beckmann, V., Rau, A., et al. 2003, A&A, 411, L299
Woods, P. M., Kouveliotou, C., van Paradijs, J., et al. 1999, ApJL, 527, L47
Yamaoka, K., Endo, A., Enoto, T., et al. 2009, PASJ, 61, S35
Zhang, B., Zhang, B.-B., Virgili, F., et al. 2009, ApJ, 703, 1696
Zhang, X.-L., Rau, A., & von Kienlin, A. 2010, in Proc. 8th INTEGRAL Workshop on The Restless Gamma-ray Universe, 2010 September 27–30, Dublin, Ireland, PoS(INTEGRAL2010)161